Design and Analysis of a New H-4 Family Parallel Manipulator

Natdanai Tantawiroon and Viboon Sangveraphunsiri

Robotics and Manufacturing Lab., Department of
Mechanical Engineering, Chulalongkorn University
254 Phya Thai, Pathum Wan, Bangkok 10330 Thailand
Tel. 0-2218-6450 Fax 0-2218-6583
E-mail: Viboon.S@eng.chula.ac.th

Abstract

This paper illustrates a novel asymmetric design of the H-4 family of parallel robots aimed at milling and Rapid-Prototyping applications with three degrees of freedom (DOF) in translation and one in rotation. The design considerations, as well as thorough analysis of forward and inverse position and velocity relationships, are presented, and a singularity analysis of the mechanism in question is also detailed. The design shows an advantage over the other conventional designs in less complexity of direct kinematics solutions, greater workspace in one selected axis and great mobility within the workspace.

Keywords: H4, Parallel Manipulator, Inverse, Forward Kinematics, Singularity

1. Introduction

At present, the researches in the robotics field have advanced dramatically. There are needs in various kinds of industries for robots that perform a variety of tasks ranging from simple pick-and-place to complex machining, effectively. The parallel robot is one of the subjects that the communities have paid great attention to for the past several years. Since Gouge and Stewart [1] proposed the earliest form of practical parallel manipulator for testing and flight simulation purposes, the research in parallel robots has continued to grow. Each link of a parallel robot is connected to the end-effecter in a parallel fashion which differs greatly from serial-link robots. The advantages of parallel manipulators over serial manipulators are high load capacity, higher stiffness and lower link inertia, while to the contrary, serial-link robots excel in large workspaces and offer more flexibility. Due to these characteristics, parallel robots are perfect for milling or coordinate measuring machines, thanks to their large capacity and rigidity. Due to the difficulties caused by the complexity of parallel robots, several researches have been devoted to closed-form forward kinematics solutions of the Stewart Platform, both analytically and computationally. The computational approach is presented in [2], [3], as well as an analytical approach in [4], [5]. In [6] and [7], redundant sensors were used to measure additional passive joint angles to help simplify the forward kinematics polynomial. Also there are numerous approaches using other algorithms such as neural networks and look-up tables to search for correct forward kinematics solutions either on-line or off-line. Thus far, there is no exact solution for the forward kinematics of the general Stewart-like parallel platform. The research aimed for discovery of efficient parallel robot configurations such as the famous Delta Robot [8] and Eclipse II [9] which can rotate 360 degree, and manipulator at the University of Maryland [10] which uses parallelogram to constrain robot motion result in 3 DOF in translation. In addition, singularity region verification is rather important, especially the singularity within the workspace. The singularity configuration of a closed chain mechanism has been thoroughly detailed in [11]. Singularity analysis is presented in various papers, by geometric approach [12-15]. A robot with adjustable parameters, such as link length

and footprint to increase working volume or avoid singularity, is presented in [16]. The early configuration of parallel robot came in the form of the Hexapod, a moving platform actuated by six actuators, which are attached to the fixed platform such as Toyada, HexaM, Giddings & Lewis, etc. Undeniably, the majority of parallel-link machines specialized in milling application nowadays, are Hexapod. As one already observed, milling processes often requires three to five DOFs, thus the Hexapod has redundancy; controlling its six actuators to perform a 5-DOF sufficient task. Some researches have been devoted to parallel robots that have less than 6-DOF such as a 3-DOF manipulators by [17] to [20]. The 5-DOF design is shown in [21]. On the contrary, lesser efforts have been devoted to 4-DOF mechanisms as in [22] and [23]. Nevertheless, the three DOFs are often not enough to carry out tasks and the six DOFs are more complex. The other approach according to this research is to develop a 4-DOF manipulator. In [23], a new family of parallel robots, called H-4, has been developed. The configuration has 3 degrees of translation and 1 degree in rotation. The design conditions of the so called mechanism are thoroughly detailed in [23]. Although lesser-than-six-DOF robots have less complex kinematics, in general forward kinematics solutions still can not be expressed in closed form, as shown in [22], which states that the forward kinematics solutions are in the form of 8^{th} order polynomials. On the contrary, the general H-4 configuration reviewed in this paper shows that there are some actuator arrangements that reduce the complexity of manipulators, thus leading to more convenient analysis of robot characteristics.

In case of working volume, one should see that parallel robots usually have a small workspace, in contrast to its large work load capacity. This can be described as "virtual reduction ratio"; the long actuators traveling distance results in a small robot end effecter movement. The in-line actuator arrangement should extend the workspace in one direction. Such arrangements, for hexapod robots with constant link length, are called "Hexaglide" [24]. In the case of 4-DOF robots, the configuration consists of two pairs of identical kinematics chain connecting to the moving platform in a manner that satisfies the closed chain DOF constraint.

In this paper, a new design has been proposed. Forward and inverse kinematics are also detailed including singularity analysis presented in analytical form. The analytical form of kinematics analysis is proved to be a powerful tool for further study of advanced parallel robot applications.

2. Design Consideration

For better understanding of the H-4 parallel robot, reader should consult [22] and [23] for more detail. From the Grübler criterion and Euler's equation:

$$F = \lambda(n - j - 1) + \sum_i f_i \tag{1}$$

$$L = j - n + 1 \tag{2}$$

Where,

- L Number of internal loops within mechanism
- F Degrees of freedom
- N Number of links including the base
- j Number of joints
- j_i Number of joints whose degrees of freedom equal i
- f_i Degrees of freedom of joint i
- λ Degrees of freedom within robot working space

Combining the two equations, in case of a parallel mechanism with four DOFs, L = 3 and F = 4. Thus, the sum of DOFs of all joints is 22. The mechanism must consist of four chains resulting in 4(5) + 2 = 22, which shows that each chain should contain five DOFs. Considering the possibilities to construct such mechanisms, except for actuated joints, the four DOFs joints are left in each chain which can be achieved with two universal joints (U joints). Two of these chains combine into one meta-chain connected to the moving platform via two revolute joints (R joints) yielding 22 joints as shown in Figure 1.

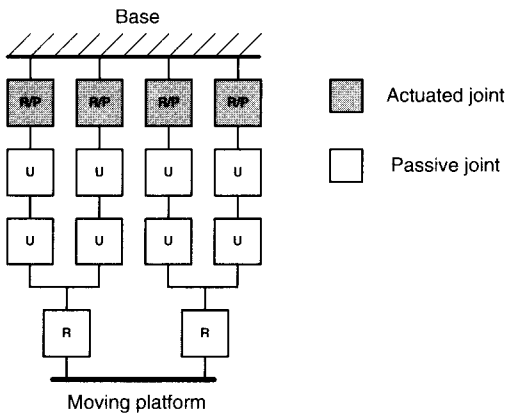

Figure 1 Possible 4-DOF parallel robot joint arrangement

The general configuration of the robot is shown in Figure 2. For milling applications, the manipulator end-effecter should point downward which is opposed to that of a classical Stewart Platform. All actuators should be fixed in place to minimize inertia effects. The actuated joint can be either revolute or prismatic joints (P joints). The following robot descriptions only apply to robots with prismatic actuators. The robots end-effecter which is called a moving platform consists of points $\mathbf{C}_{12}$, $\mathbf{C}_{34}$ and $\mathbf{P}$ as shown in Figure 2. The platform can rotate in the direction of v. The machine consists of four actuators $\mathbf{A}$ with the length of l_1, l_2, l_3 and l_4 with respecte to the coordinate frame {D}.

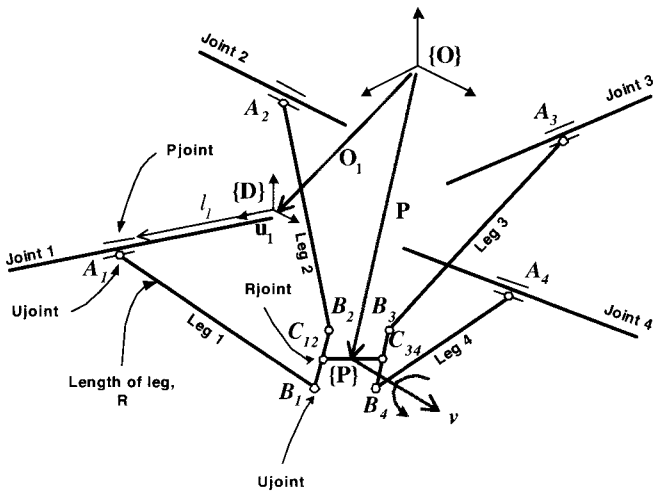

Figure 2 General configuration of the 4-DOF parallel robot

Where,

- **{O}** Robot origin frame
- **P** Position vector of robot moving platform described as $\{x, y, z\}^T$
- l_i Actuated linear joint i length
- v Rotation vector of moving platform
- **{P}** Coordinate frame attached to moving platform
- **{D}** Coordinate frame attached to actuated joint
- $\mathbf{u}_i$ Unit vector pointed in actuator direction
- $\mathbf{O}_i$ Constant vector due to robot construction and origin frame placement

Starting with the inverse kinematics problem, the solution l_i is found for i = 1 to 4, for each desired robot position $\{x, y, z\}^T$ and θ.

As can be seen, with simple vectors addition for leg i:

$$\mathbf{O}_i + \mathbf{l}_i + \mathbf{A}_i\mathbf{B}_i = \mathbf{C}_i\mathbf{B}_i + \mathbf{P} + \mathbf{Rot}(\mathbf{v},\theta)\bullet\mathbf{PC}_i$$
$$\mathbf{A}_i\mathbf{B}_i = \mathbf{P} - \mathbf{l}_i + \mathbf{Rot}(\mathbf{v},\theta)\bullet\mathbf{PC}_i + \mathbf{C}_i\mathbf{B}_i - \mathbf{O}_i \quad (3)$$

$\mathbf{Rot}(v,\theta)$ is the rotation matrix in the direction of v for the amount of θ. Vector $\mathbf{l}_i$ can be written as $\mathbf{l}_i = l_i\mathbf{u}_i$ and all constant vectors can be combined to be $\mathbf{K}_i = \mathbf{C}_i\mathbf{B}_i - \mathbf{O}_i$ thus (3) can be rewritten as:

$$R\left[\frac{\mathbf{A_iB_i}}{\|\mathbf{A_iB_i}\|}\right]=\mathbf{P}-l_i\mathbf{u_i}+\mathbf{Rot(v},\theta)\bullet\mathbf{PC_i}+\mathbf{K_i}, \quad (4)$$

$$R\left[\frac{\mathbf{A_iB_i}}{\|\mathbf{A_iB_i}\|}\right]=\begin{bmatrix}x+[\mathbf{Rot(v},\theta)\bullet\mathbf{PC_i}]_x+[\mathbf{K_i}]_x\\ y+[\mathbf{Rot(v},\theta)\bullet\mathbf{PC_i}]_y+[\mathbf{K_i}]_y\\ z+[\mathbf{Rot(v},\theta)\bullet\mathbf{PC_i}]_z+[\mathbf{K_i}]_z\end{bmatrix}-l_i\begin{bmatrix}u_{ix}\\ u_{iy}\\ u_{iz}\end{bmatrix} \quad (5)$$

Vector $\mathbf{C_iB_i}$ is, $\mathbf{C_{12}B_1}$ for leg 1, and $\mathbf{C_{12}B_2}$ for leg 2, respectively. The same can be applied to leg 3 and 4 to yield vectors $\mathbf{C_{34}B_3}$ and $\mathbf{C_{34}B_4}$. Subscripts x, y and z refer to corresponding vector components along the x, y and z axes.

The typical approach is to square both sides of the equation, thus change three rows of matrix into one scalar equation. This can hardly be done, because $\mathbf{l_i}$ has all components in x, y and z directions. We can reduce $\mathbf{u_i}$ into $[1\ 0\ 0]^T$ by rotating **{O}** so that $\mathbf{u_i}$ coincides with the x axis. This rotation matrix, according to Figure 3, is found to be:

$$\mathbf{R_i}=\begin{bmatrix}\mathbf{u_i^T}\\ \mathbf{v_i^T}\\ \mathbf{w_i^T}\end{bmatrix}$$

$$\mathbf{w_i}=\frac{\mathbf{i}\times\mathbf{u_i}}{\|\mathbf{i}\times\mathbf{u_i}\|},\ \mathbf{v_i}=\mathbf{w_i}\times\mathbf{u_i} \quad (6)$$

Where,

$\mathbf{R_i}$ Rotation matrix that transforms coordinate frame **{O}** to coordinate frame **{D}** of actuator i

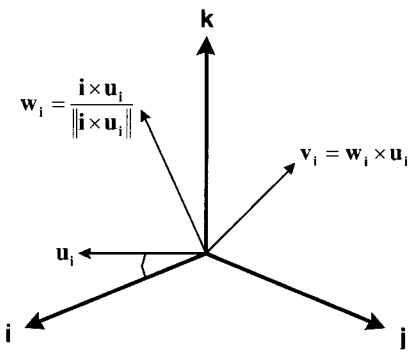

Figure 3 Rotating {O} to make x coincide with u_i Hence,

$$\mathbf{R_i}R\left[\frac{\mathbf{A_iB_i}}{\|\mathbf{A_iB_i}\|}\right]=\mathbf{R_i}\begin{bmatrix}x+[\mathbf{Rot(v},\theta)\bullet\mathbf{PC_i}]_x+[\mathbf{K_i}]_x\\ y+[\mathbf{Rot(v},\theta)\bullet\mathbf{PC_i}]_y+[\mathbf{K_i}]_y\\ z+[\mathbf{Rot(v},\theta)\bullet\mathbf{PC_i}]_z+[\mathbf{K_i}]_z\end{bmatrix}-l_i\mathbf{R_i}\begin{bmatrix}u_{ix}\\ u_{iy}\\ u_{iz}\end{bmatrix}$$

$$\mathbf{R_i}R\left[\frac{\mathbf{A_iB_i}}{\|\mathbf{A_iB_i}\|}\right]=\begin{bmatrix}u_{ix}\cdot x_i+u_{iy}\cdot y_i+u_{iz}\cdot z_i\\ v_{ix}\cdot x_i+v_{iy}\cdot y_i+v_{iz}\cdot z_i\\ w_{ix}\cdot x_i+w_{iy}\cdot y_i+w_{iz}\cdot z_i\end{bmatrix}-l_i\begin{bmatrix}1\\0\\0\end{bmatrix}$$

$$\mathbf{R_i}R\left[\frac{\mathbf{A_iB_i}}{\|\mathbf{A_iB_i}\|}\right]=\begin{bmatrix}u_{ix}\cdot x_i+u_{iy}\cdot y_i+u_{iz}\cdot z_i-l_i\\ v_{ix}\cdot x_i+v_{iy}\cdot y_i+v_{iz}\cdot z_i\\ w_{ix}\cdot x_i+w_{iy}\cdot y_i+w_{iz}\cdot z_i\end{bmatrix} \quad (7)$$

Where,

$$\begin{bmatrix}x+[\mathbf{Rot(v},\theta)\bullet\mathbf{PC_i}]_x+[\mathbf{K_i}]_x\\ y+[\mathbf{Rot(v},\theta)\bullet\mathbf{PC_i}]_y+[\mathbf{K_i}]_y\\ z+[\mathbf{Rot(v},\theta)\bullet\mathbf{PC_i}]_z+[\mathbf{K_i}]_z\end{bmatrix}=\begin{bmatrix}x_i\\ y_i\\ z_i\end{bmatrix} \quad (8)$$

Now we can solve for linear joint length, l_i for actuator i as follows:

$$R^2\left\|\mathbf{R_i}\left[\frac{\mathbf{A_iB_i}}{\|\mathbf{A_iB_i}\|}\right]\right\|^2=\left\|\begin{matrix}u_{ix}\cdot x_i+u_{iy}\cdot y_i+u_{iz}\cdot z_i-l_i\\ v_{ix}\cdot x_i+v_{iy}\cdot y_i+v_{iz}\cdot z_i\\ w_{ix}\cdot x_i+w_{iy}\cdot y_i+w_{iz}\cdot z_i\end{matrix}\right\|^2$$

$$l_i=u_{ix}\cdot x_i+u_{iy}\cdot y_i+u_{iz}\cdot z_i\pm\sqrt{R^2-\left(v_{ix}\cdot x_i+v_{iy}\cdot y_i+v_{iz}\cdot z_i\right)^2-\left(w_{ix}\cdot x_i+w_{iy}\cdot y_i+w_{iz}\cdot z_i\right)^2} \quad (9)$$

Noting that $\mathbf{R_i^TR_i=I}$

At this point, readers can see that the arrangement of actuated joint direction, **l** plays an important role in defining the characteristics of the robot [20].

The situation is more complicated in the case of forward kinematics, as has already been pointed out by the others [2, 3, and 4]. For simplification, for each meta-chain, points **B** and **C** can be seen as the same point. The configuration in Figure 2 reveals that point $\mathbf{C_{12}}$ and $\mathbf{C_{34}}$ can only move in a circular path; movement of leg $\mathbf{A_1B_1}$ and $\mathbf{A_2B_2}$ forms two spheres where the intersection of these spheres is the path of $\mathbf{C_{12}}$. The same can applied to $\mathbf{C_{34}}$ resulting in two circles which are perpendicular to and positioned at the midpoint of vector $\mathbf{A_1A_2}$ and $\mathbf{A_3A_4}$, respectively. Obviously, the radius of the circles is dependent on both linear joint

lengths at each side of the closed chain. The solutions to the forward kinematics problem are where the points $\mathbf{C_{12}}$ and $\mathbf{C_{34}}$ satisfy the following conditions:

1. Size of $\mathbf{C_{12}C_{34}}$ is equal to the size of the moving platform and,
2. Dot product of $\mathbf{C_{12}C_{34}}$ and v is a constant. Depending on the selection of point **C**, the vector v keeps its original direction and $\mathbf{C_{12}C_{34}}$ always rotates around v. The angle between $\mathbf{C_{12}C_{34}}$ and v is also a constant. It is more convenient to select **C** such that $\mathbf{C_{12}C_{34}}$ is perpendicular to v, thus $\mathbf{C_{12}C_{34}} \bullet v = 0$

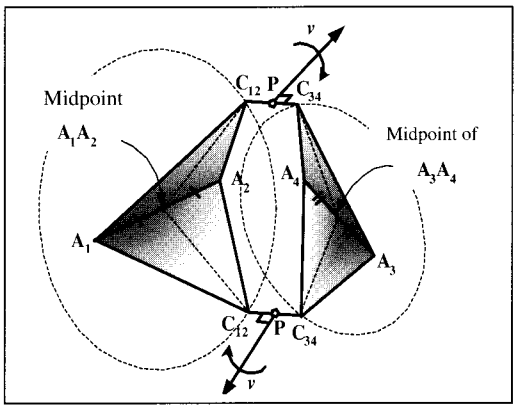

Figure 4 Multiple forward kinematics solutions

As shown in Figure 4, these circles may or may not intersect with each other. Thus, They produce four but not more than eight solutions [22].

3. Proposed Design

From the above discussion, the H-4 family parallel mechanism is presented as in Figure 5. The machine consists of four actuators l_1, l_2, l_3 and l_4 which point in the x direction according to the machine origin. Four legs **AB** of length R comprise the PUU joints. Leg 1 and leg 2 are designated by $\mathbf{A_1B_1}$ and $\mathbf{A_2B_2}$ and leg 3 and leg 4 are designated by $\mathbf{A_3B_3}$ and $\mathbf{A_4B_4}$ and form the meta-chain (independent closed chain) at each side, They are connected to the moving platform via two revolute joints at **C** resulting in rotation in the y direction. From the kinematics point of view, if we set vector **l** so that it coincides with one of the principle axis, which in this case is x, equation (9) can be simplified. This approach not only simplifies the expression but also extends the robot workspace in that direction. Furthermore, if we align $\mathbf{l_1}$ with $\mathbf{l_2}$ and $\mathbf{l_3}$ with $\mathbf{l_4}$, the constant vector $\mathbf{K_i}$ for leg 1 and 2 and for leg 3 and 4 will be identical. Thus, this makes actuator 1 align with actuator 2 as well as actuator 3 and 4. Also, the moving path of point $\mathbf{C_i}$ will become circular in the plane perpendicular to $\mathbf{l_i}$ as shown in Figure 6. As mentioned before, the origin and radius of the circle are constrained by actuated linear joint lengths l_1 and l_2 for $\mathbf{C_{12}}$ and l_3 and l_4 for $\mathbf{C_{34}}$.

Designing parameters include leg length (R), the difference between platform size and footprint (A-B), platform size (C) and meta-chain offset distance (D). Parameters determination depends on a number of factors, resulting in optimization of mechanism characteristics such as stiffness and working volume.

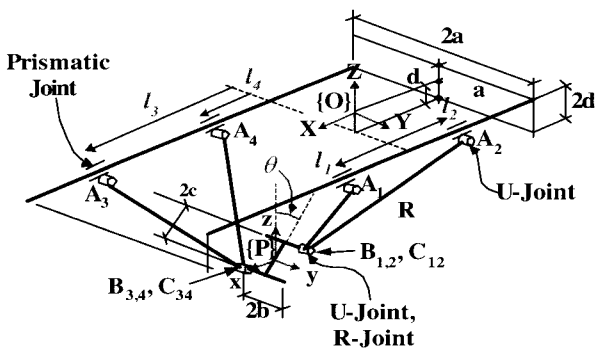

Figure 5 Configuration of proposed manipulator

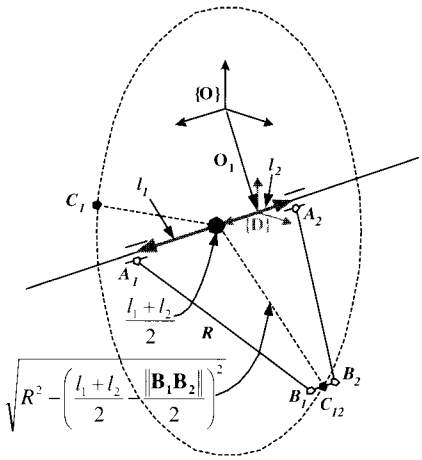

Figure 6 Detail of actuated linear joint length l_1 and l_2 which are related to the path of point C_{12}

3.1 Inverse Kinematics

Consider Figure 5 and equation (8) and (9) from section 2 and the beginning of section 3 given:

$$\mathbf{O}_1 = \mathbf{O}_2 = [0 \quad a \quad d]^T$$

$$\mathbf{C}_{12}\mathbf{B}_1 = \mathbf{C}_{12}\mathbf{B}_{12} = \mathbf{0}$$

$$\mathbf{PC}_{12} = [0 \quad b \quad c]^T$$

In the same manner:

$$\mathbf{O}_3 = \mathbf{O}_4 = [0 \quad -a \quad -d]^T$$

$$\mathbf{C}_{34}\mathbf{B}_3 = \mathbf{C}_{34}\mathbf{B}_4 = \mathbf{0}$$

$$\mathbf{PC}_{34} = [0 \quad -b \quad -c]^T$$

Furthermore:

$$\mathbf{u}_i = [1 \quad 0 \quad 0]^T, \mathbf{R}_i = \mathbf{I}, i = 1-4$$

And for rotation in the y direction:

$$\mathbf{Rot}(v,\theta) = \begin{bmatrix} \cos(\theta) & 0 & \sin(\theta) \\ 0 & 1 & 0 \\ -\sin(\theta) & 0 & \cos(\theta) \end{bmatrix}$$

Substitute all this into equation (9) and this yields.

$$l_1 = x + c\sin(\theta) \pm \sqrt{R^2 - (y+b-a)^2 - (z + c\cos(\theta) - d)^2}$$

From the geometric configuration of robot, there is only one solution which is:

$$l_1 = x + c\sin(\theta) + \sqrt{R^2 - (y+b-a)^2 - (z + c\cos(\theta) - d)^2} \tag{10}$$

$$l_2 = x + c\sin(\theta) - \sqrt{R^2 - (y+b-a)^2 - (z + c\cos(\theta) - d)^2} \tag{11}$$

$$l_3 = x - c\sin(\theta) + \sqrt{R^2 - (y-b+a)^2 - (z - c\cos(\theta) + d)^2} \tag{12}$$

$$l_4 = x - c\sin(\theta) - \sqrt{R^2 - (y-b+a)^2 - (z - c\cos(\theta) + d)^2} \tag{13}$$

From equations (10) to (13), one can solve for actuated linear joint length for any given platform position.

3.2 Forward kinematics analysis

From robot input parameters l_1, l_2, l_3 and l_4 we assume new variables depending on these inputs to be:

$$r_1 = \frac{l_1 + l_2}{2}, r_2 = \frac{l_3 + l_4}{2}$$
$$d_1 = l_1 - l_2, d_2 = l_3 - l_4 \tag{14}$$

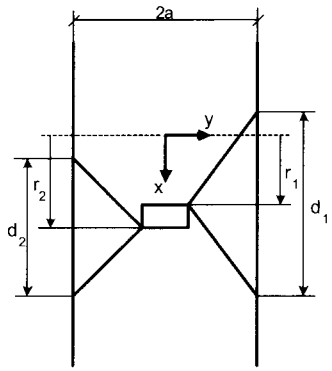

Figure 7 New variables assignment as observe from the top of the manipulator

Which can be described as (see also Figure 5):

r_1, r_2 Origin of the circular path of vector **C**

d_1, d_2 Distance between $\mathbf{A_1}$ and $\mathbf{A_2}$ and between $\mathbf{A_3}$ and $\mathbf{A_4}$

By the geometric approach, the rotation of the platform can readily be determined as:

$$\cos(\theta) = \frac{\sqrt{4c^2 - (r_1 - r_2)^2}}{2c} \tag{15}$$

Noting that point $\mathbf{C_{12}}$ of closed chain 1-2 is always above $\mathbf{C_{34}}$ of chain 3-4. Thus, the range of θ is within ±90 degree about y axis. Equation (15) shows that cos(θ) is always positive for θ within the first and fourth quadrants.

The solution in the x direction is easily obtained as:

$$x = \frac{r_1 + r_2}{2} \tag{16}$$

The detail of the solutions is shown in Figure 8.

Here, we can independently acquire two of four forward kinematics solutions. As for motion along the y and z axis, manipulating equations (10) to (13) yield y in the form of z in two independent equations as shown below:

$$y = \frac{d_1^2 - d_2^2 + 8z\left[\sqrt{4c^2 - (r_2 - r_1)^2} - 2d\right]}{16(a-b)} \tag{17}$$

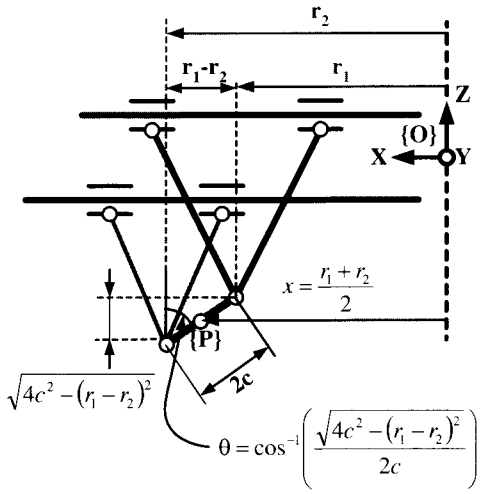

Figure 8 Determining x and θ from robot geometry

$$\frac{d_1^2 + d_2^2}{4} = 2R^2 - 2y^2 - 2(b-a)^2 - 2z^2 - 2(c\cdot\cos(\theta) - d)^2 \tag{18}$$

Substituting equation (18) into (17) results in a 2nd order polynomial of z which can be solved using a simple formula:

$$z = \frac{-B \pm \sqrt{B^2 - 4AC}}{2A} \tag{19}$$

Where

$$A = \frac{\left[\sqrt{4c^2 - (r_2 - r_1)^2} - 2d\right]^2}{2(a-b)^2} + 2$$

$$B = \frac{(d_1^2 - d_2^2)\left[\sqrt{4c^2 - (r_2 - r_1)^2} - 2d\right]}{8(a-b)^2}$$

$$C = \frac{d_1^2 + d_2^2}{4} - 2R^2 + 2(b-a)^2 + \frac{1}{2}\left[\sqrt{4c^2 - (r_2 - r_1)^2} - 2d\right]^2 + \frac{(d_1^2 - d_2^2)^2}{128(a-b)^2} \tag{20}$$

Due to the configuration of the proposed robot, the solution in z is always negative.

3.3 Jacobian Analysis

The velocities relationship matrix can be obtained using direct derivatives of kinematics relations that are already obtained or by manipulating kinematics relations between links and moving platform. In the following sections, we will concentrate on the design proposed. The Jacobian or the matrices which relate input joints velocity to that of robot position is in the form:

$$\partial \mathbf{F}(\mathbf{q},\mathbf{x}) = \mathbf{0}$$

In other words,

$$\mathbf{A}\dot{\mathbf{q}} + \mathbf{B}\dot{\mathbf{x}} = \mathbf{0}, \tag{21}$$

Where,

- $\dot{\mathbf{q}}$ The velocity of actuated joints, $[\dot{l}_1, \dot{l}_2, \dot{l}_3, \dot{l}_4]^T$
- $\dot{\mathbf{x}}$ Velocity of robot moving platform, $\dot{\mathbf{x}} = [\dot{x}, \dot{y}, \dot{z}, \dot{\theta}]^T$
- $\mathbf{F}(\mathbf{q},\mathbf{x}) = \mathbf{0}$ The position relationships between actuated joints and robot position
- **A** Derivative of **F** with respect to **q**, $\partial \mathbf{F}/\partial \mathbf{q}$
- **B** Derivative of **F** with respect to **x**, $\partial \mathbf{F}/\partial \mathbf{x}$

Thus, the Jacobian can be expressed in the form:

$$\mathbf{J} = -\mathbf{A}^{-1}\mathbf{B}, \tag{22}$$

Consider other forms of equation (10),

$$F(l_1,\mathbf{x}) = (x + c\sin(\theta) - l_1)^2 + (y + b - a)^2 + (z + c\cos(\theta) - d)^2 - R^2 = 0 \tag{10}$$

Thus,

$$\partial F / \partial l_1 = -2(x + c\sin(\theta) - l_1)\cdot \dot{l}_1$$

And,

$$\partial F / \partial x = 2(x + c\sin(\theta) - l_1)\cdot \dot{x}$$

$$\partial F / \partial y = 2(y + b - a)\cdot \dot{y}$$

$$\partial F / \partial z = 2(z + c\cos(\theta) - d)\cdot \dot{z}$$

$$\partial F / \partial \theta = 2c(x + c\sin(\theta) - l_1)\cos(\theta)\cdot\dot{\theta} - 2c(z + c\cos(\theta) - d)\sin(\theta)\cdot\dot{\theta}$$

Repeating and combining the operations for actuators 2, 3 and 4 give:

$$\mathbf{A} = -\begin{bmatrix} x + c\cdot\sin(\theta) - l_1 & 0 & 0 & 0 \\ 0 & x + c\cdot\sin(\theta) - l_2 & 0 & 0 \\ 0 & 0 & x - c\cdot\sin(\theta) - l_3 & 0 \\ 0 & 0 & 0 & x - c\cdot\sin(\theta) - l_4 \end{bmatrix}$$

$$\mathbf{B} = \begin{bmatrix} x + c\cdot\sin(\theta) - l_1 & y + b - a & z + c\cdot\cos(\theta) - d & c\left((x + c\cdot\sin(\theta) - l_1)\cos(\theta) - (z + c\cdot\cos(\theta) - d)\sin(\theta)\right) \\ x + c\cdot\sin(\theta) - l_2 & y + b - a & z + c\cdot\cos(\theta) - d & c\left((x + c\cdot\sin(\theta) - l_2)\cos(\theta) - (z + c\cdot\cos(\theta) - d)\sin(\theta)\right) \\ x - c\cdot\sin(\theta) - l_3 & y - b + a & z - c\cdot\cos(\theta) + d & c\left(-(x - c\cdot\sin(\theta) - l_3)\cos(\theta) + (z - c\cdot\cos(\theta) + d)\sin(\theta)\right) \\ x - c\cdot\sin(\theta) - l_4 & y - b + a & z - c\cdot\cos(\theta) + d & c\left(-(x - c\cdot\sin(\theta) - l_4)\cos(\theta) + (z - c\cdot\cos(\theta) + d)\sin(\theta)\right) \end{bmatrix}$$

$$\mathbf{J} = \begin{bmatrix} 1 & \dfrac{y + b - a}{x + c\cdot\sin(\theta) - l_1} & \dfrac{z + c\cdot\cos(\theta) - d}{x + c\cdot\sin(\theta) - l_1} & c\left(\cos(\theta) - \dfrac{(z + c\cdot\cos(\theta) - d)\sin(\theta)}{x + c\cdot\sin(\theta) - l_1}\right) \\ 1 & \dfrac{y + b - a}{x + c\cdot\sin(\theta) - l_2} & \dfrac{z + c\cdot\cos(\theta) - d}{x + c\cdot\sin(\theta) - l_2} & c\left(\cos(\theta) - \dfrac{(z + c\cdot\cos(\theta) - d)\sin(\theta)}{x + c\cdot\sin(\theta) - l_2}\right) \\ 1 & \dfrac{y - b + a}{x - c\cdot\sin(\theta) + l_3} & \dfrac{z - c\cdot\cos(\theta) + d}{x - c\cdot\sin(\theta) + l_3} & c\left(-\cos(\theta) + \dfrac{(z - c\cdot\cos(\theta) + d)\sin(\theta)}{x - c\cdot\sin(\theta) + l_3}\right) \\ 1 & \dfrac{y - b + a}{x - c\cdot\sin(\theta) + l_4} & \dfrac{z - c\cdot\cos(\theta) + d}{x - c\cdot\sin(\theta) + l_4} & c\left(-\cos(\theta) + \dfrac{(z - c\cdot\cos(\theta) + d)\sin(\theta)}{x - c\cdot\sin(\theta) + l_4}\right) \end{bmatrix}$$

(23), (24) and (25)

Matrices (23) to (25) represent velocity relationships between actuators and the moving platform.

3.4 Singularity Analysis

Singularity analysis is of paramount important in parallel kinematics due to their complex linkage nature. The situation where singularity occurs was described in [1], and the Jacobian matrix was outlined in three cases as follows:

Singularity of the 1st kind arises when **det(A)** is zero, because there exists a non-zero vector $\dot{\mathbf{q}}$ which makes the output velocity $\dot{\mathbf{x}}$ zero. This means that the manipulator loses its one or more end-effecter DOF or refers to where the multiple branches of the inverse kinematics solutions meet. This type of singularity does not impose serious difficulties because it is actually encountered at the boundary of the working volume. Singularity of the 2nd kind is encountered when **det(B)** is zero, which are the points where there is end effecter motion. Input actuator velocities are zero when the multiple branches of forward kinematics solutions meet. In this case, the manipulator gains one or more uncontrollable DOF which can be encountered within the workspace, which results in unexpected behavior. Singularity of the 3rd kind is a special case which occurs when both determinants of **A** and **B** are zero, and depends on robot parameters such as link length.

To keep the article organized, the detailed procedure to obtain the determinant of both matrices will not be shown here.

In case of **A**, its determinant is:

$$\det(\mathbf{A}) = (x + c\cdot\sin(\theta) - l_1)(x + c\cdot\sin(\theta) - l_2)(x - c\cdot\sin(\theta) - l_3)(x - c\cdot\sin(\theta) - l_4) \quad (26)$$

These imply that, singularity occurs when $x \pm c\sin(\theta) - l_1 = 0$ or, as shown in Figure 9a, when leg 1 and 2 or leg 3 and 4 become parallel. Consider Figure 6b, the radius of circular path of **C** is maximized when leg 1 and 2 become parallel, which clearly designates the working boundary of the robot.

As for **B**, due to the likeliness of matrix rows, by performing row and column operation, one can obtain the determinant of **B** as:

$$\det(\mathbf{B}) = 4c\cdot(l_1 - l_2)\cdot(l_3 - l_4)\cdot\cos(\theta)\cdot[y(d - c\cdot\cos(\theta)) - z(b - a)] \quad (27)$$

Observing the determinant of **B** reveals that the singularity occurs at the following conditions;

1. At $l_1 = l_2$ or $l_3 = l_4$ which means that vector $\mathbf{A_1B_1}$ with $\mathbf{A_2B_2}$ together with $\mathbf{A_3B_3}$ and $\mathbf{A_4B_4}$ are coincided as shown in Figure 9a. This is similar to condition (26) but when legs in the same closed chain are parallel, the chain becomes an open chain and gains more DOF. From observation, point **C** can move spherically and the robot becomes unstable.
2. At $\cos(\theta) = 0$ or $\theta = \pm 90°$ where the platform is parallel to x as shown in Figure 9b.
3. The position where planes formed by $\mathbf{A_1B_1}$ with $\mathbf{A_2B_2}$ and $\mathbf{A_3B_3}$ with $\mathbf{A_4B_4}$ are in parallel as shown in Figure 9c and can be described by the expression,

$$y(d - c\cdot\cos(\theta)) - z(b - a) = 0$$
$$z = \frac{y(d - c\cdot\cos(\theta))}{(b - a)}$$

It is also important to note that although the singularity condition can be avoided mathematically, in real manufacturing conditions, all tolerances and mating conditions must be considered carefully. Joint clearance can accumulate and make a greater impact on the stability of the robot, most importantly, near the singularity region. In conclusion, the singularity region should be avoided with significant safety factor.

The proposed manipulator design kinematics properties can be shown in analytical form which can be used to analyze the characteristics of the manipulator efficiently.

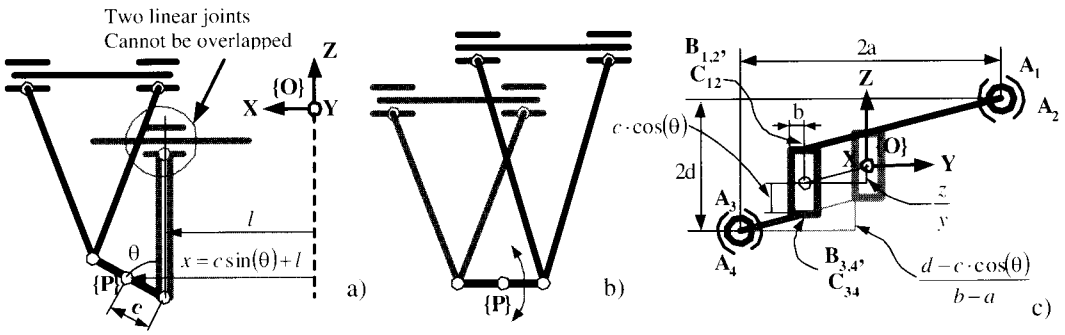

Figure 9 Possible singularity configurations a) Legs in one or both meta-chain are parallel b) Moving Platform has rotated ±90° and c) Plane $A_1A_2B_{12}$ and $A_3A_4B_{34}$ are parallel as observed from the front

3.5 Workspace

From the previous analysis, the workspace of manipulator strongly depends on robot design parameters. The design parameters include robot footprint (a-b), platform size (c), meta-chain offset distance (d) and leg length (R). Varying this sets of parameters affects the characteristics of the robot such as workspace and stiffness. Thanks to its simple configuration along the x axis, the workspace of the robot is the area constructed from the permitted movement of point **C** on each side of the chain. The boundary is achieved by keeping the distance between actuated joint $\mathbf{A_1}$ and $\mathbf{A_2}$ or $\mathbf{A_3}$ and $\mathbf{A_4}$ at the minimum (d_{min}) (i.e. each leg is nearly parallel) and varying the other side from the maximum (d_{max}) to the minimum as shown in Figure 10. From the above discussion, singularity d_{max} must be less than twice R and also d_{min} must be larger than zero. The following plot varies d_{max} in the range of 1.3R to 1.7R and d_{min} from 0.5R to 0.6R.

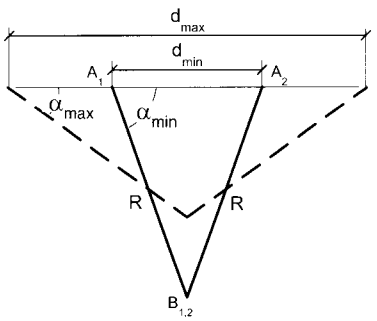

Figure 10 Maximum and minimum allowable traveling distance of robot actuators

In this proposed design, only workspace in the yz plane is considered. Figures 11a to 11d show the workspace in yz plane where θ = 0° for each set of parameters, for Figure 11a: c = d = 0.1, R = 0.4; Figure 11b: (a-b) = 0.14, c =d = 0.2: Figure 11c: (a-b) = 0.14, R = 0.4: and Figure 11d: (a-b) = 0.14, R = 0.4, c = 0.02. As can be seen in Figure 11a, increasing the footprint of the robot will decrease the workspace in both y and z directions. On the contrary, as in Figure 11b, increasing the leg length tends to increase the workspace in the yz plane.

The variation of the workspace due to the rotation of the moving platform along the y axis is investigated. As shown in Figure 11c, the workspace shows good mobility of platform for platform angle as large as 60 degrees, observed from only slight drift from the neutral position (position of arm when the moving platform angle is at 0 degree) in the yz plane workspace. The workspace shifts away from the neutral position more when the platform angle, as the well as platform size increases. As far as c = d, as in Figure 11c, the neutral position remains in the center; the workspace is symmetric to the y = 0 axis. In case c is not equal to d, as in Figure11d, the neutral position shifts to both sides of the y = 0 axis depending on which parameter is larger. Noting that, from singularity analysis, decreasing the footprint and increasing the length the of the robot's leg give more workspace, but likely push the robot into singularity.

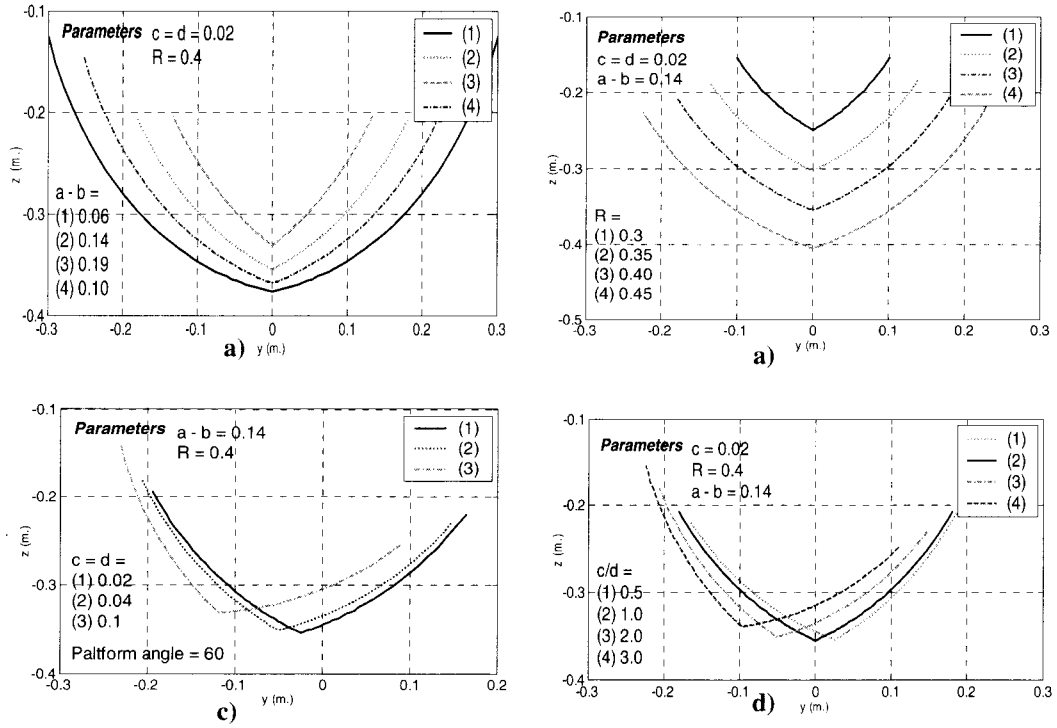

Figure 11 Workspace of robot in the yz plane varying parameters a) Varying robot base size (a-b), when the platform angle is 0 degree (neutral position) b) Varying leg length R, at the neutral position c) Varying platform size c, and the meta-chain offset distance d, when the platform angle is 60 degree and d) Varying the ratio of c and d, at the neutral position (all plots taken from Matlab/Simulink® R6.1)

4. Simulation results

The simulation based on the derived kinematics relation using Matlab/Simulink® for control law implementation and MSC.virtual Nastran® for numerical plant simulation are shown. The simulation performed both, controlling each joint directly, and tracking pre-generated platform trajectory. The block diagram is shown in Figure 12. As for joints control, we assign PID-control with position feedback for each individual joint. In the case of tracking platform trajectory, we generate the path for the platform motion using linear and parabolic blending, in addition to a control signal consisting of position, velocity feedback and integral term. For the ideal case, the actual moving platform trajectory should exactly match the desired trajectory with no error, given the control law:

$$\mathbf{F} = \mathbf{K}_P(\mathbf{l} - \mathbf{l}_d) + \mathbf{K}_D(\dot{\mathbf{l}} - \dot{\mathbf{l}}_d) + \mathbf{K}_I \int (\mathbf{l} - \mathbf{l}_d)dt$$

$$\mathbf{F} = \mathbf{K}_P\mathbf{e} + \mathbf{K}_D\dot{\mathbf{e}} + \mathbf{K}_I \int \mathbf{e}dt \qquad (28)$$

Where

- $\mathbf{l}_d$ Desired joints position
- $\mathbf{l}$ Actual joints position
- $\dot{\mathbf{l}}_d$ Desired joints velocity
- $\dot{\mathbf{l}}$ Actual joints velocity
- $\mathbf{K}_P$ Proportional gain
- $\mathbf{K}_D$ Derivative gain
- $\mathbf{K}_I$ Integral gain
- $\mathbf{e}$ Tracking error
- $\mathbf{F}$ Control signal

By assigning the conditions as:
Start point:

$$x = -0.01\ y = -0.016\ z = -0.467\ \theta = 29^\circ$$

End point:

$$x = -0.1\ y = -0.05\ z = -0.38\ \theta = 0^\circ$$

Figure 13 and Figure 14 show the simulation results of the positions and velocities of the moving platform, Figure 13, and of the actuated joints, Figure 14, controlling the joints directly. The simulation results illustrate this very promising control scheme.

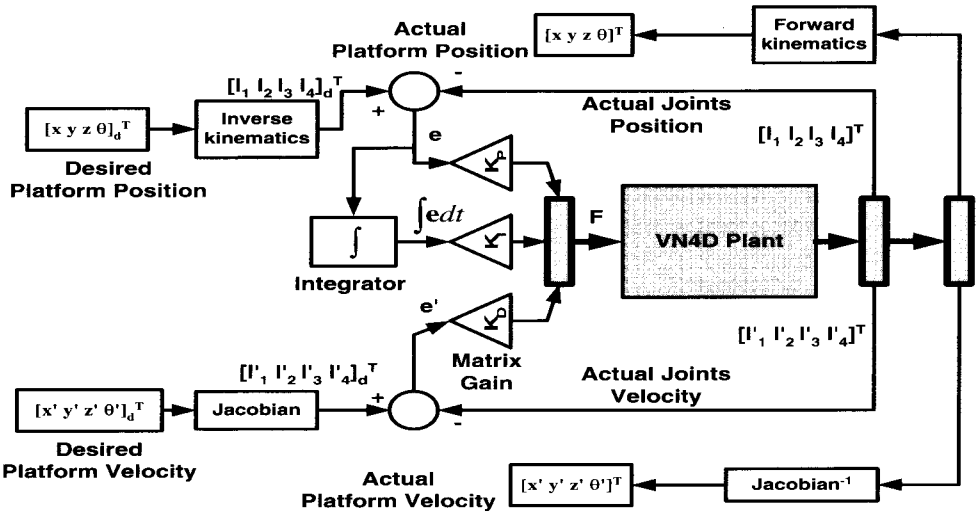

Figure12 Block diagram of manipulator PID control system

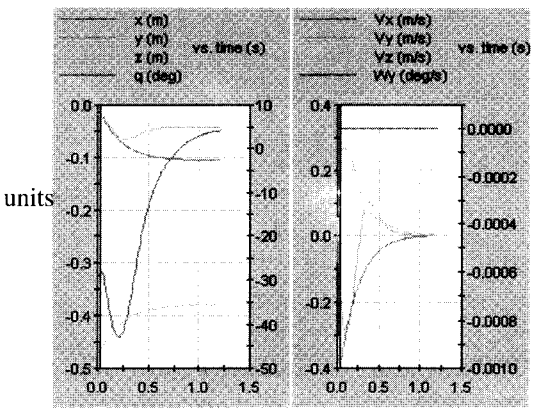

Figure 13 Positions and velocities of the moving platform by controlling each joint directly

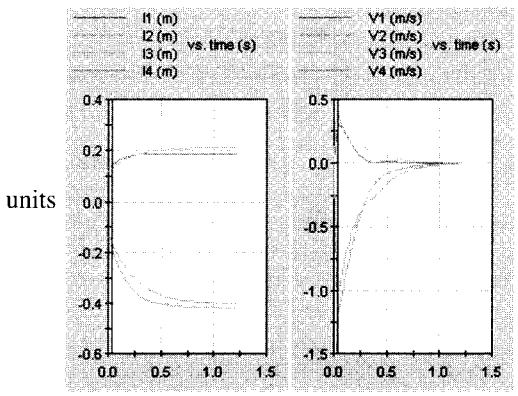

Figure 14 Positions and velocities of the actuated joints by controlling each joint dirctly

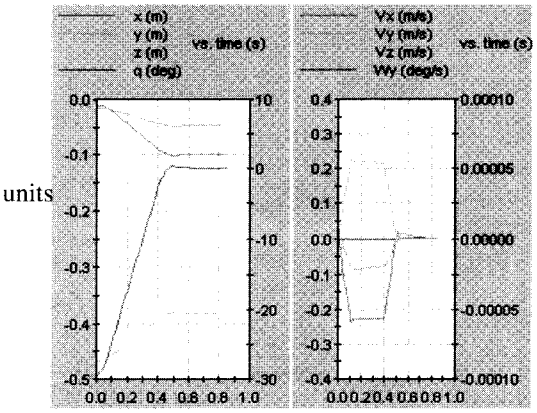

Figure 15 Positions and velocities tracking of the moving platform using pre-generated path.

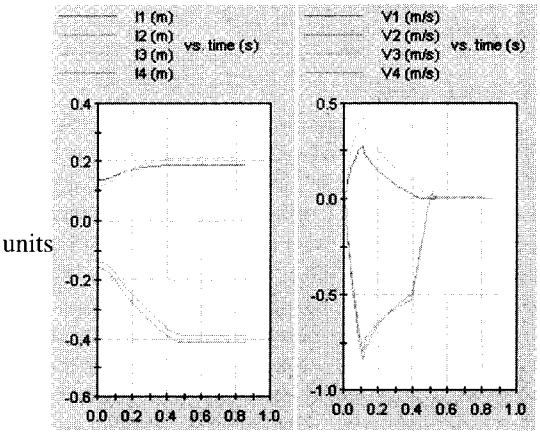

Figure 16 Positions and velocities tracking of the actuated joints using pre-generated path.

Similarly, by controlling the platform path, Figure 15 and 16 show the simulation results of the positions and velocities of the moving platform and of the actuated joints. By using the joint PID-control, the same results can be obtained.

Figure 17 shows the acceleration of the platform. This is similar to the acceleration of the trapezoidal velocity profile. Also, the maximum platform velocity of 0.2 m/s with 0.3g in acceleration, is also shown.

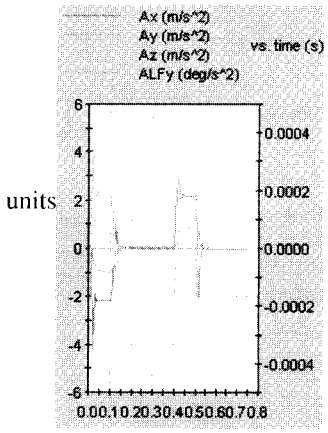

Figure 17 Acceleration of the Platform using Cartesian space control scheme.

At present, a prototype arm was built as shown in Figure 18. The test bed is useful for further research, as a device to perform force tracking control on surfaces, and as a small milling machine for rapid prototyping applications.

5. Conclusions

In this paper, extensive analysis of the new H-4 family parallel manipulator has been presented. The inverse kinematics and especially forward kinematics can be represented in closed form. Singularity analysis is also shown in analytical form thanks to its simple design. The robot provided good work space in the x direction and good mobility all around for the working volume. A robot control simulation, using both joint space and Cartesian space, has been carried out. The results show good characteristics and controllability of the manipulator.

6. Acknowledgement

The author wishes to thank Chulalongkorn University for supporting the research under the HM 72nd anniversary research assisting fund.

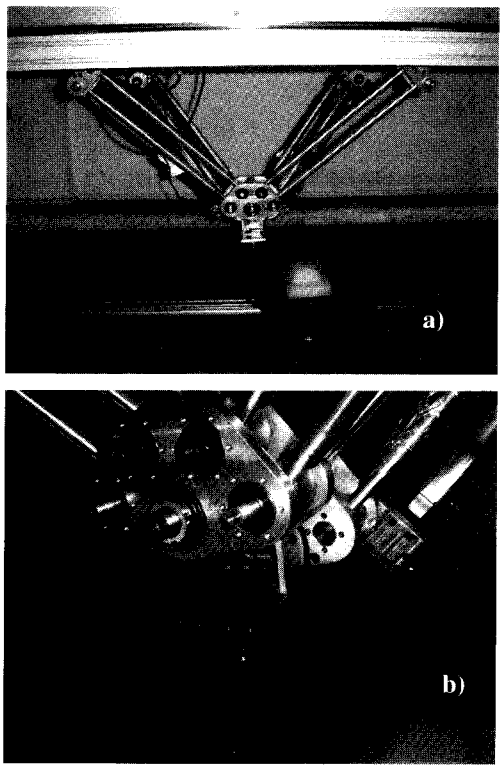

Figure18 a) The prototype robot arm and b) Detail of the moving platform and revolute joints

7. References

[1] Stewart, D., A Platform with 6 Degrees of Freedom., Proc. Institution of Mechanical Engineers, 180 (part 1, 15, pp. 371-386), 1965.

[2] Sang, L.H., Han, M.C., The Estimation for Forward Kinematics Solution of Stewart Platform Using the Neural Network. Proc. IEEE/RSJ, International Conference on Intelligent Robots and System, pp.1501-1506, 1999.

[3] Yee C.S. and Lim K.B. Neural Network for the Forward Kinematics Problem in Parallel Manipulator. Proc. IEEE, Int. Joint Conf. on Neural Network, Singapore, pp.1699-1704, 1991.

[4] Lazard, D., Merlet, J.P., The (true) Stewart Platform has 12 Configurations, Proc. IEEE, International Conference on Robotics & Automation, pp.2160-2165, 1994.

[5] Stoughton, R. Arai, Y., Optimal Sensor Placement for Forward Kinematics Evaluation of a 6-dof Parallel Link Manipulator, IEEE/RSJ, International Workshop on Intelligent Robots and Systems, Osaka Japan, pp.785-790, 1991.

[6] Merlet, J.P., Closed-form Resolution of the Direct Kinematics of Parallel Manipulators Using Extra Sensors Data., Proc., IEEE, International Conference on Robotics and Automation, Vol.1, pp.200 -204, 1993.

[7] Chiu, Y.J., Perng, M.H., Forward Kinematics of a General Fully Parallel Manipulator with Auxiliary Sensors. International Journal of Robotics Research, Vol.20, No.5, pp.401-414, 2001.

[8] Clavel, R., Conception D'un robot Parallèle Rapide à 4 Degrés Deliberté, Doctoral Dissertation Thesis, EPFL, Lausanne, Switzerland, 1991.

[9] Kim, J., Eclipse-II: a New Parallel Mechanism Enabling Continuous 360-Degree Spinning Plus Three-axis Translational Motions, Proc. IEEE, International Conference on Robotics & Automation, Seoul, Korea, pp.3274-3279, 2001.

[10] Tsai, L.W., Walsh, G.C., Stamper, R.E., Kinematics of a Novel Three DOF Translational Platform, Proc. IEEE International Conference on Robotics & Automation, Minneapolis, Minnesota, pp.3447-3451, 1996.

[11] Gosselin, C., Angeles, J., Singularity Analysis of Closed-loop Kinematics Chains. IEEE Transactions on Robotics & Automation, Vol. 6, No.3, pp.959-968, 1990.

[12] Angeles, J., Yang, G. et al, Singularity Analysis of Three-legged Parallel Robots Based on Passive-joint Velocities. Proc. IEEE International Conference on Robotics & Automation, Seoul, Korea, pp.2407-2412, 2001.

[13] Angeles, J., Yang, G. et al, Singularity Analysis of Three-legged, Six-DOF platform Manipulators with RRRS Legs, Proc. IEEE, International Conference on Advances Intelligent Mechatronics, Como, Italy, pp. 32-36, 2001.

[14] Monsarrat, B., Gosselin, C., Singularity Analysis of a Three-Leg 6 DOF parallel Grassmann Line Geometry, International Journal of Robotics Research, Vol.20, No.4, pp.312-326, 2001.

[15] Lee, M.K., Park, K.W., Workspace and Singularity Analysis of a Double Parallel Manipulator, IEEE/ASME Transactions on Mechatronics, Vol.5, No.4, pp.367-375, 2000.

[16] Arai, T. et al, Parallel mechanisms with Adjustable Link Parameters. Proc. IEEE/RSJ International Conference on Intelligent Robots and Systems, pp.671-676, 2000.

[17] Liu, X.J. et al., On the Analysis of a New Spatial Three-degrees-of-freedom Parallel Manipulator, IEEE, Transactions on Robotics & Automation. Vol. 17, No.6, pp. 959-968, 2001.

[18] Liu, X.J., Kim, J., A New Three-degrees-of-freedom Parallel Manipulator, Proc. IEEE, International Conference on Robotics & Automation, Washington, DC, pp.1155-1160, 2002.

[19] Tsai, L.W., Joshi, S., Comparison Study of Architectures of Four 3 Degrees-of-freedom Translational Parallel Manipulators, Proc. IEEE, International Conference on Robotics & Automation, Seoul, Korea, pp.1283-1288, 2001.

[20] Tsai, L.W., Joshi, S., A Comparison Study of To 3-DOF Parallel Manipulators: One with Tree and the Other with Four Supporting legs, Proc. IEEE, International Conference on Robotics & Automation, Washington, DC, pp.3690-3697, 2002.

[21] Li, C., Huang, Z., Type Synthesis of 5-DOF Parallel Manipulator, Proc. IEEE, International Conference on Robotics & Automation, Taipei, Taiwan, pp.1203-1208, 2003.

[22] Company, O., Marquet, F., Pierrot, F., A New High-Speed 4-DOF Parallel Robot Synthesis and Modeling Issues, IEEE, Transactions on Robotics and Automation, Vol.19, No.3, pp.411-420, 2003.

[23] Pierrot, F., Marquet, F., H4 Parallel Robot Modeling Design and Preliminary Experiments, International Conference on

IEEE Robotics and Automation, Seoul Korea, pp.3256-3261, 2001.

[24] Honegger, M. et al, Adaptive Control of the Hexaglide, a 6 DOF Parallel Manipulator. Proc. IEEE, International Conference on Robotics and Automation, Albuquerque, New Mexico, p.543-548, 1997.